IEEE Open Access Journal of
Power and Energy

Received 15 September 2023; revised 30 December 2023; accepted 27 January 2024.
Date of publication 31 January 2024; date of current version 13 February 2024.

Digital Object Identifier 10.1109/OAJPE.2024.3360854

Systematic Decoupling Grid-Forming Control for Utility-Scale Inverter-Based Distributed Energy Resources in Weak Distribution Grids

LINA HE (Senior Member, IEEE), AND SHIWEN YU (Graduate Student Member, IEEE)

Department of Electrical and Computer Engineering, University of Illinois at Chicago, Chicago, IL 60607 USA

CORRESPONDING AUTHOR: L. HE (lhe@uic.edu)

ABSTRACT Existing grid-forming inverter control schemes for distributed energy resources (DERs) primarily rely on active power (P)-frequency (f) and reactive power (Q)-voltage (V) droop mechanisms that are tailored for highly inductive transmission grids. However, in weak distribution grids where P and Q are highly coupled due to their resistive network characteristics, these control schemes cannot provide independent and accurate f and V regulation. This will further deteriorate the dynamic and stability performance, potentially resulting in inverter and load tripping during disturbances. To address this challenge, this paper proposes an innovative decoupling grid-forming control scheme, which is designed based on a systematic perspective that considers the inherent coupling characteristic of the entire distribution grid. The small-signal stability of the proposed controller is analyzed by varying controller parameters and the grid strength. The effectiveness of this controller is comprehensively verified using both MATLAB and OPAL-RT platforms by comparing it with existing grid-forming control strategies. The results show that the proposed controller can effectively decouple P and Q regulation in weak distribution grids. It enables DERs to provide independent, accurate, and autonomous f and V regulation, thus improving grid stability and dynamics. The proposed control strategy is cost-effective, communication-free, and can be easily commercialized due to its straightforward and robust circuit design.

INDEX TERMS Decoupling control, grid-forming, utility-scale DERs, weak distribution grids, frequency and voltage regulation.

NOMENCLATURE

Acronyms

DER	Distributed energy resource.
P	Active power.
f	Frequency.
Q	Reactive power.
V	Voltage.
PV	Photovoltaic.
PLL	Phase-locked loop.
EV	Electric vehicle.
FRT	Fault ride-through.
PCC	Point of common coupling.
SCR	Short circuit ratio.
Z_{DER}	Output impedance of DER.
p.u.	Per unit.

I. INTRODUCTION

UNDER strong clean energy incentives, such as "100% carbon-free electricity by 2035" of the U.S. power sector [1], the conventional electricity network is rapidly transitioning into a more distributed structure to facilitate the widespread integration of renewable DERs [2]. These DERs are usually integrated into distribution grids via inverters, which introduce numerous power electronic components and greatly decrease the system inertia [3]. The resulting low inertia can significantly reduce the strength of the grid, making it vulnerable to voltage instability and frequency oscillations. Operational challenges and instability issues of inverter-based resources in weak transmission grids have been documented globally. Notable examples include reports from the ERCOT [4] and AEMO [5]. These issues can result

in severe consequences, such as device damage and even widespread power outages, exemplified by the 2016 South Australia blackout [5] and the 2019 United Kingdom blackout [6]. Similar risks are present in weak distribution grids with high penetration of DERs and less rotating mass [7], [8].

In response, the IEEE 1547 Standard provides critical guidelines for DER integration, emphasizing the need for effective f and V regulation in distribution grids [9]. Meanwhile, there is a notable surge in research focusing on f and V regulation in distribution grids. In [10], the effects of employing thermostatically controlled loads for f regulation in distribution grids are studied, which reveals increased risks in V variations and transformer aging. Multiple f and V regulation techniques such as grid-forming and grid-supporting converter controls are comprehensively reviewed in [11]. It particularly focuses on modified control strategies for inductive, resistive, and general line types. In [12], the use of energy storage systems for f regulation in power systems is investigated based on a bi-level optimization model with chance constraints and a decentralized algorithm. However, economic factors are not extensively covered. In [13], an online V regulation method for active distribution grids is discussed using a deep neural encoding-decoding approach. It is designed to overcome the complexities of traditional mixed-integer quadratic programming by using an offline encoding process that simplifies the problem into quadratic programming and an online decoding process using a deep neural network. In [14], a step control reactive power strategy for V regulation is presented for unbalanced power systems with residential photovoltaics (PVs). It can effectively manage V unbalance and overvoltage. However, the long-term integration challenges should be comprehensively addressed.

To avoid these risks, it is urgent for DERs, especially those at the utility-scale, to have grid-forming capabilities. These capabilities play a crucial role in regulating the f and V of the power grid to ensure its stability, reliability, and resilience [15]. Grid-forming control schemes have been demonstrated to enhance damping in comparison to traditional grid-following control schemes. This enhancement becomes increasingly vital as the penetration level of inverters increases, contributing to sustained reliable system operation and optimal dynamic performance.

Existing commercial DERs usually operate as grid-following sources that act as passive P and Q controlled sources. They merely regulate their power output by following the grid angle/frequency via a phase-locked loop (PLL), yet they fall short in providing constructive f and V support for weak grids [16], [17]. In contrast, DERs that employ grid-forming control schemes, such as droop control [18], virtual synchronous generator control [19], and virtual oscillator control [20], act as autonomous voltage sources. They are independent of the PLL and can actively regulate their output f and V, which enables them to operate as synchronous generators and stabilize the system. Among these grid-forming control methods, droop control is extensively utilized to address challenges such as harmonics, power sharing, and system instability due to the integration of DERs. A coordinated virtual impedance control scheme using sequence-based droop control and virtual impedance is presented to enhance the integration of electric vehicles (EVs) with the power grid [21]. It can effectively improve harmonics mitigation and power quality under both balanced and unbalanced events. In [22], a control method for AC/DC hybrid microgrids based on dual converters is discussed. This control aims to enhance grid-tied performance, operational transitions, and power sharing in islanded modes. Droop control can be integrated into a hierarchical control framework that addresses reactive and harmonic power sharing, especially in islanded microgrids [23], [24], [25], [26]. In [27], a controller using droop control and virtual resistance is reported. It aims to provide advanced services such as fault ride-through (FRT) [28]. However, these studies focus on the inverter side system viewed from the point of common coupling (PCC) and neglect the influence of the grid-side characteristics on controller dynamics. Factors such as the grid strength and coupling issue of P and Q are not taken into account.

Besides, the other two existing grid-forming control methods exhibit inherent limitations. For instance, virtual synchronous generator control schemes replicate the inertia and droop characteristics of synchronous generators to achieve f and V control [19]. However, this approach does not fully exploit the rapid response capabilities of inverters and may adversely affect system dynamics. Additionally, virtual oscillator control schemes have emerged in recent years, aiming to emulate a nonlinear oscillator with a natural frequency aligned with the grid frequency. These schemes are designed to provide support for both frequency and voltage, although they are still in the early stages of development [20]. Although these control methods exhibit distinct dynamic performances owing to their unique characteristics, they share a commonality in regulating inverter output with a similar steady-state response, as they all adhere to the droop law [29]. It is known that droop-based control is traditionally designed for highly inductive transmission grids where f and V are decoupled due to a high reactance-to-resistance (X/R) ratio [15]. However, this design can lead to instability in scenarios with wide variations in grid impedance X/R ratios and associated power coupling issues. In weak distribution grids with resistive characteristics and coupled P and Q, existing grid-forming control schemes based on the droop mechanism encounter challenges in achieving independent and effective f and V regulation [30].

Addressing the coupling of P and Q is crucial for effective f and V regulation, as well as for resolving stability and dynamic issues in DER control. The work in [31] and [32] uses modified droop functions that consider both P and Q in voltage and/or frequency regulations. However, they do not sufficiently address the decoupling of P and Q based on grid characteristics in their controller designs [31], [32]. Specif-

ically, the study in [31] applied a P-Q-V droop controller, which uses both P and Q to regulate the output voltage. However, the coupling coefficient of the P and Q in this study is assumed to be a constant, i.e., 1, which is unrealistic for most distribution grids, thus failing to accurately reflect real-world coupling characteristics [15]. In addition, it neglects the coupling of P and Q in f control. Another droop controller based on P-V and Q-(-δ) is discussed in [33]. It aims to ensure stable parallel operation of diverse inverter types, facilitating accurate load sharing and improved stability. However, it is important to note that this control method is tailored for a passive load rather than a power grid, which may limit its responsiveness to changes in grid dynamics.

Additional approaches involve DER output impedance (Z_{DER})-based decoupling control methods, including virtual impedance-based and virtual frame-based grid-forming control methods [34], [35]. The virtual impedance-based control integrates a large virtual inductor into the control loop to compensate for the resistance of the outlet distribution line connecting the inverter to the PCC [34]. However, this method will compromise the stability margin and may decrease the system damping. The virtual frame control uses a transformation frame in the inverter control to build a virtual f and V frame, aiming to decouple the output P and Q of the DER [35]. Nevertheless, these methods primarily address the coupling issue at the DER system level, including the filter and outlet line, without considering the coupling of P and Q on the grid side. This oversight can lead to severe instability issues in real-world power systems with significant grid impedance variations due to varying grid structures and strength.

Recent studies have shed light on how grid-side characteristics significantly impact control dynamics [36], [37], [38], [39]. In [36], the exploration of control stability under varying grid impedance conditions highlights the instability risks of grid-connected inverters, particularly in scenarios of high grid impedance. Reference [37] analyzes the small-signal stability of power inverters and the impedance characteristics of power systems. The impedance behavior of two-stage photovoltaic inverters is investigated in [38], demonstrating how power inverter dynamics can lead to instability, especially in weak grids with a high R/X ratio. Additionally, [39] explores the sensitivity of inverter-based resources to grid line impedance, especially in residential applications. This study underscores the necessity for sophisticated control strategies that take into account the coupling relationship between P and Q of the grid side.

Special consideration should be given to weak distribution grids with complex grid-side characteristics. A weak distribution grid is defined as having a lower short circuit ratio (SCR) of less than 3 and an X/R ratio of less than 5 [40]. These grids typically exhibit low inertia and are susceptible to voltage and frequency instability. Furthermore, weak distribution grids are characterized by a low X/R ratio, resulting in a significant coupling issue of P and Q. They usually have a larger grid impedance compared to the DER system and cannot be neglected in inverter controller design. Consequently, the Z_{DER}-based decoupling control schemes discussed in [33] and [34] are unable to enable utility-scale DERs to provide independent and effective f and V regulation. The reason is that these schemes treat the power grid as an ideal Thevenin equivalent circuit and neglect the inherent coupling issue of weak distribution grids. As a result, this oversight might exacerbate vulnerabilities of such weak grids, posing threats to system stability and resilience. Thus, addressing the coupling issue of P and Q on the grid side is essential to prevent severe instability in power systems, particularly those facing large grid impedance variations due to diverse grid structures and strengths.

To overcome these challenges, this paper proposes a novel, comprehensive, and systematic decoupling grid-forming control scheme based on the widely used droop control. The droop control is more appealing than other grid-forming control methods due to its basic simplicity and fast-response characteristics. The proposed control considers not only the inverter and its associated components but also the power grid with intricate power coupling characteristics. Unlike existing decoupling methods that primarily focus on the circuit of the inverter and its associated components, our approach rigorously incorporates the grid-side dynamics, addressing the challenges introduced by the high R/X ratio of weak distribution grids. This holistic design philosophy is based on an innovative systematic decoupling of P and Q, enhancing the dynamic performance and stability of the power grid with distributed energy resources. It introduces a significant advancement in grid-forming control strategies, providing a more robust and adaptive solution for next-generation distribution grids with a high penetration of DERs.

Specifically, the proposed control strategy aims to decouple P and Q of weak distribution grids in real time by extracting their coupling characteristics online and designing an adaptive grid-forming decoupler. This allows DERs to provide independent f and V regulation, thereby enhancing system resilience. The proposed grid-forming controller is cost-effective and easily commercializable due to its simple and robust circuit design. Additionally, as a grid-forming control, the strategy operates autonomously on local measurements, eliminating the need for communication. It is universally applicable to all DERs, reducing communication costs and minimizing vulnerability to cyber-attacks. The performance of the proposed control technique is thoroughly validated using a detailed weak distribution grid model based on the IEEE 14 bus system through comprehensive MATLAB and OPAL-RT simulation. The results demonstrate that the proposed control can independently regulate f and V by decoupling P and Q online. It exhibits superior stability, steady-state, and dynamic performance when compared to existing grid-forming control strategies. To the best knowledge of the authors, this paper represents the first

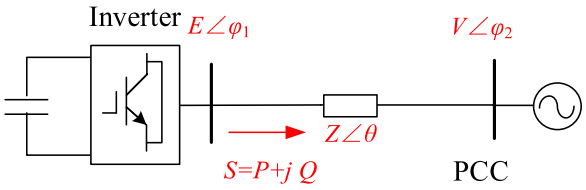

FIGURE 1. Traditional equivalent grid-connected DER system for control design.

comprehensive exploration of systematic decoupling control for inverters in weak distribution grids.

The organization of the remaining sections in this paper is outlined as follows. Section II derives the coupling characteristics of the power grid and introduces the systematic decoupling grid-forming controller. Section III formulates the small-signal model of the proposed controller, along with detailing the parameter design with consideration of the stability analysis. Section IV provides the simulation scenarios and corresponding results. Finally, Section V serves as the conclusion for the paper.

II. PROPOSED SYSTEMATIC DECOUPLING GRID-FORMING CONTROL

The proposed systematic decoupling grid-forming control is designed based on the coupling characteristics of the weak distribution grid, as derived in this section.

A. TRADITIONAL DROOP CONTROL MECHANISM

Traditional inverter control design considers the power grid as an ideal voltage source at the PCC, as shown in Fig. 1 [17], [18], [19], [20].

The P and Q transmitted from the inverter to the grid can be represented by the voltages at the inverter terminal and the PCC, along with the impedance between these two points, as shown in (1) and (2).

$$P = \frac{EVsin\varphi}{Z}\sin\theta + \frac{E(E - Vcos\varphi)}{Z}\cos\theta \tag{1}$$

$$Q = -\frac{EVsin\varphi}{Z}\cos\theta + \frac{E(E - Vcos\varphi)}{Z}\sin\theta \tag{2}$$

where P and Q denote the output active and reactive power of the DER, respectively; E and V denote the magnitudes of the inverter terminal voltage and PCC voltage, respectively. The parameter φ represents the phase angle difference between the inverter terminal voltage and PCC voltage (obtained from $\varphi_1 - \varphi_2$); while $Z\angle\theta$ represents the output impedance of the DER system, comprising the impedances of the filter and outlet line.

In high-voltage transmission grids, the impedance $Z\angle\theta$ in Fig. 1 is typically highly inductive ($\theta \approx 90°$) due to the high X/R ratio of the transmission line. In addition, the phase angle difference φ is usually negligible. As a result, under the assumptions of $\sin\theta \approx 1$, $\cos\theta \approx 0$, $sin\varphi \approx \varphi$, and $cos\varphi \approx 1$, (1) and (2) can be simplified, resulting in (3) and (4) [12].

$$P = \frac{EV\varphi}{Z} \tag{3}$$

$$Q = \frac{E\,(E - V)}{Z} \tag{4}$$

As seen, when the magnitudes of the PCC voltage and line impedance are fixed, a linear relationship is observed both between P and φ and between Q and E. This linearity facilitates the applicability of droop characteristics in grid-forming inverter control within transmission systems. Specifically, these relationships can be represented as (5) and (6) [14] and [18].

$$f^* = f_0 - m(P_{mea} - P_0) \tag{5}$$

$$E^* = E_0 - n(Q_{mea} - Q_0) \tag{6}$$

where f^* and E^* represent the generated references of frequency and amplitude of the inverter terminal voltage, and f_0 and E_0 denote their rated values; P_{mea} and Q_{mea} are the measurements of the output active and reactive power; P_0 and Q_0 are the setpoints based on the dispatched active and reactive power, indicating the output power of the inverter at nominal frequency f_0 and nominal voltage magnitude E_0; m and n represent the positive coefficients of P-f and Q-E droop slopes, respectively. Note that the P-f droop scheme is used instead of the P-φ droop scheme, as the f reference can be easily fixed at nominal values, while the initial phase angle of the PCC voltage cannot be known by the inverter [41].

However, the assumptions inherent in droop control are limited to highly inductive transmission grids. In medium or low-voltage distribution grids, which are predominantly resistive and weak, these assumptions lose their validity. As a result, traditional droop-based control becomes incapable of independently regulating f and V by adjusting P and Q respectively. The underlying reasons are outlined below:

1) For a distribution line, its power flow equations (1) and (2) cannot be simplified to (3) and (4) due to its low X/R ratio. As a result, the output P and Q of inverters become coupled and associated with the f and V.
2) A weak distribution grid typically exhibits a high grid impedance, so it cannot be treated as an ideal voltage source, as depicted in Fig. 1. Moreover, the resistive dominant characteristics of the high grid impedance result in interdependence between f and V control due to the coupling of P and Q. Therefore, the weak distribution grid and its associated impacts should not be overlooked in inverter control design.

In weak distribution grids, the coupling issue can lead to significant mutual interference between f and V control in DERs. In extreme situations, this interference may result in system instability, severe device damage, or even widespread outages.

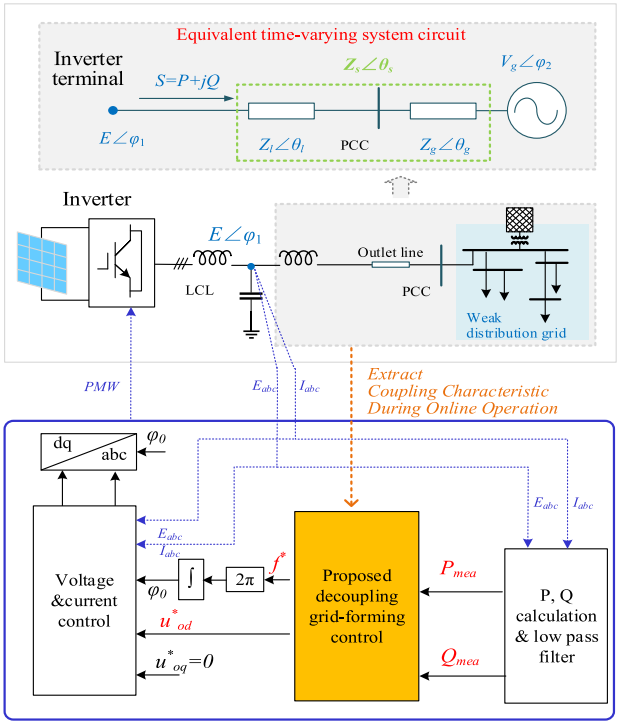

FIGURE 2. Systematic decoupling grid-forming control system.

B. PROPOSED SYSTEMATIC DECOUPLING GRID-FORMING CONTROL

To overcome this challenge, this paper proposes a systematic decoupling grid-forming control scheme. This scheme aims to decouple the inverter output P and Q with consideration of the comprehensive coupling characteristic of the power grid. It enables DERs to independently control f and V in weak distribution grids and improve dynamic performance. The configuration of the proposed control scheme is shown in Fig. 2. As depicted, a DER system is connected to a weak distribution grid via an LCL filter and an outlet distribution line. The node between the two inductors of the filter is viewed as the inverter terminal and its voltage and current measurements are utilized as input signals for the control system (depicted in the blue frame). This control system is composed of three main components: (1) a P and Q calculation block with low-pass filters; (2) the proposed outer-loop decoupling grid-forming controller; and (3) an inner-loop voltage and current controller.

The proposed systematic decoupling grid-forming control is designed to decouple the entire resistive-dominated system, encompassing the weak distribution grid, the DER filter, and the outlet distribution line. The coupling characteristics of the entire grid are continuously monitored and utilized to determine the control parameters in real-time. The derivation of the coupling characteristic and the controller design are discussed in the subsequent sections.

To identify the coupling characteristic of the entire integrated grid, this paper develops an equivalent circuit model of the system viewed from the inverter terminal, as illustrated in Fig. 2. Different from the model in Fig. 1, this equivalent circuit showed in Fig. 2 consists of two time-varying components: a time-varying impedance $Z_s\angle\theta_s$ and a time-varying voltage source $V_g\angle\varphi_2$. These components reflect the online dynamics of the studied weak system and can be determined online based on real-time measurements during system operation. $Z_s\angle\theta_s$ represents the total system impedance as seen from the inverter terminal. It is the sum of three parts, including the filter impedance on the system side, the impedance of the outlet distribution line, and the equivalent impedance of the weak distribution grid. The first two parts are readily determined based on the parameters of the inverter and distribution line provided by DER and utility operators. The equivalent impedance of the weak distribution grid can be identified online by monitoring the voltage and current variations at the PCC during events like load changes, as shown in (7).

$$Z_g\angle\theta_g = \frac{\vec{V}_1 - \vec{V}_2}{\vec{I}_1 - \vec{I}_2} \tag{7}$$

where $\vec{V}_1$ and $\vec{I}_1$ represent the pre-event measurements of voltage and current phasors, respectively, while $\vec{V}_2$ and $\vec{I}_2$ represent the post-event measurements. By applying KVL, the equivalent grid voltage $V_g\angle\varphi_2$ can be deduced using $\vec{V}_2$ and $Z_g\angle\theta_g$, as shown in (8).

$$V_g\angle\varphi_2 = \vec{V}_2 - Z_g\angle\theta_g * \vec{I}_2 \tag{8}$$

Based on the developed equivalent time-varying system circuit, the combined system impedance, including both the output impedance and grid impedance, is determined in (9).

$$Z_s\angle\theta_s = Z_l\angle\theta_l + Z_g\angle\theta_g \tag{9}$$

where

$$Z_s = \sqrt{Z_l^2 + Z_g^2} \tag{10}$$

$$\theta_s = \tan^{-1}\frac{Z_l\sin\theta_l + Z_g\sin\theta_g}{Z_l\cos\theta_l + Z_g\cos\theta_g} \tag{11}$$

Due to its resistive nature, the impedance $Z_s\angle\theta_s$ cannot be simplified with the assumptions $\sin\theta_s \approx 1, \cos\theta_s \approx 0$. However, in distribution grids, where the phase angle difference φ_s between the inverter terminal voltage ($E\angle\varphi_1$) and the grid equivalent voltage ($V_g\angle\varphi_2$) is typically small [41], the assumptions $sin\varphi_s \approx \varphi_s$ and $cos\varphi_s \approx 1$ remain valid. Thus, based on (1) and (2), the P and Q output of the DER in the weak distribution grid can be represented as (12) and (13).

$$P_s = \frac{EV_g\varphi_s}{Z_s}\sin\theta_s + \frac{E(E-V_g)}{Z_s}\cos\theta_s \tag{12}$$

$$Q_s = -\frac{EV_g\varphi_s}{Z_s}\cos\theta_s + \frac{E(E-V_g)}{Z_s}\sin\theta_s \tag{13}$$

where P_s and Q_s are active and reactive power of the DER, respectively, and V_g represents the voltage magnitude of the equivalent voltage source of the grid. From (12) and (13),

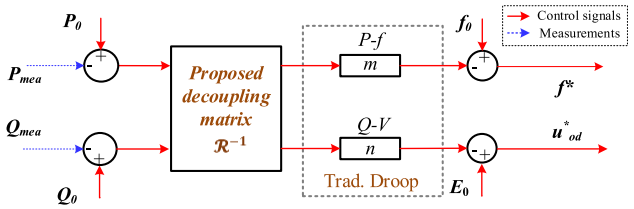

FIGURE 3. **Proposed systematic decoupling grid-forming control.**

the coupling characteristic of the system can be succinctly expressed by the matrix $\mathcal{R} = \begin{bmatrix} \sin\theta_s & \cos\theta_s \\ -\cos\theta_s & \sin\theta_s \end{bmatrix}$. To decouple the P_s and Q_s, equation (11) is multiplied by the inverse of R, i.e., $\mathcal{R}^{-1} = \begin{bmatrix} \sin\theta_s & -\cos\theta_s \\ \cos\theta_s & \sin\theta_s \end{bmatrix}$, resulting in (14).

$$\begin{bmatrix} P_d \\ Q_d \end{bmatrix} = \begin{bmatrix} \sin\theta_s & -cos\theta_s \\ \cos\theta_s & \sin\theta_s \end{bmatrix} \begin{bmatrix} P_s \\ Q_s \end{bmatrix} = \begin{bmatrix} \frac{EV_g\varphi_s}{Z_s} \\ \frac{E(E-V_g)}{Z_s} \end{bmatrix} \tag{14}$$

where $\mathcal{R}^{-1}$ is the decoupling matrix, and P_d and Q_d represent the decoupled P_s and Q_s, respectively. Notable, P_d exhibits linearity with respect to φ_s, while Q_d displays linearity with respect to E, aligning with the characteristics of the droop law, similar to (3) and (4). Consequently, the droop control can be effectively implemented by harnessing P_d and Q_d, representing the decoupled P_s and Q_s. As a result, this insight guides the design of the systematic decoupling grid-forming controller, as shown in Fig. 3, comprising a decoupler and a traditional droop controller. Specifically, the decoupler is designed based on the decoupling matrix $\mathcal{R}^{-1}$.

As shown in Fig. 3, the inputs to the proposed systematic decoupling grid-forming controller are the measured P and Q, i.e., P_{mea} and Q_{mea}, which are generated from the P and Q calculation block. The outputs of this controller are the generated frequency and voltage references for the inner-loop voltage and current controller. In Fig. 2, the frequency reference, i.e., f^*, is converted into the angle reference φ_0 for the inner loop. The generated voltage reference is viewed as the d-axis voltage reference u^*_{od} of the voltage control loop. The q-axis voltage reference, i.e., u^*_{oq}, is set to be 0.

The proposed controller in Fig. 3 can be represented mathematically as (15) and (16),

$$f^* = f_0 - mD_1\,(P_0 - P_{mea}) - mD_3\,(Q_0 - Q_{mea}) \tag{15}$$
$$E^* = E_0 - nD_2\,(P_0 - P_{mea}) - nD_4\,(Q_0 - Q_{mea}) \tag{16}$$

The decoupler parameters ($D_1 \sim D_4$) are determined based on the decoupling matrix $\mathcal{R}^{-1}$, as shown in (17).

$$\begin{cases} D_1 = \sin\theta_s \\ D_2 = \cos\theta_s \\ D_3 = -\cos\theta_s \\ D_4 = \sin\theta_s \end{cases} \tag{17}$$

It shows that the decoupler parameters mainly depend on the system impedance angle, i.e., θ_s, which can be determined during online operation as previously discussed in (9). Simultaneously, the droop parameters can be determined based on the power-sharing capability of the DER with consideration of the system stability, which is discussed in the following section. This design introduced a novel control technique that effectively address the limitations inherent in existing grid-forming control schemes. It empowers DERs to autonomously decouple the P and Q of the entire power grid, achieving independent grid-forming f and V control. This capability enables a more precise and responsive regulation of the grid, thereby enhancing stability and efficiency in various operating conditions. Importantly, this design equips DERs to dynamically adapt to the time-varying conditions of the power grid, ensuring continue stable and efficient operation. The resulting enhanced control mechanism facilitates independent and accurate frequency and voltage regulation, playing a pivotal role in fortifying the reliability and resilience of modern distribution systems.

III. SMALL-SIGNAL STABILITY ANALYSIS AND PARAMETER DESIGN

The small-signal model of the proposed controller is derived in this section. This model is utilized to analyze the small-signal stability and determine the control parameters.

A. SMALL-SIGNAL MODEL

The small-signal model is constructed through the linearization of the power transfer functions in (12) and (13). In addition, it incorporates the models of the proposed systematic decoupling grid-forming controller and the low-pass filters used for power measurement. The resulting representation of the small-signal model is expressed by (18) and (19).

$$\Delta P_s = \frac{1}{Z_s}\left[\left(EV_g\Delta\varphi + \Delta EV_g\varphi\right) sin\theta_s + \Delta E(2E - V_g)cos\theta_s\right] \tag{18}$$

$$\Delta Q_s = \frac{1}{Z_s}\left[-\left(EV_g\Delta\varphi + \Delta EV_g\varphi\right) cos\theta_s + \Delta E\left(2E - V_g\right) sin\theta_s\right] \tag{19}$$

where the prefix Δ denotes a small deviation in the variables defined in (12) and (13). Incorporating the decoupler in (14), the small-signal model is transformed into (20) and (21).

$$\Delta P_d = \begin{bmatrix} \sin\theta_s & -\cos\theta_s \end{bmatrix} \begin{bmatrix} \Delta P_s \\ \Delta Q_s \end{bmatrix} = \frac{1}{Z_s}\left(EV_g\Delta\varphi + \Delta EV_g\varphi\right) \tag{20}$$

$$\Delta Q_d = \begin{bmatrix} \cos\theta_s & \sin\theta_s \end{bmatrix} \begin{bmatrix} \Delta P_s \\ \Delta Q_s \end{bmatrix} = \frac{1}{Z_s}\Delta E(2E - V_g) \tag{21}$$

Subsequently, by modeling the droop control with low-pass filters as a first-order inertia element and substituting $\Delta\varphi$ with $2\pi\Delta f/s$, the small-signal model of the studied system can be expressed as (22) and (23).

$$\Delta f = -\frac{mw_f}{Z_s(w_f + s)}\left(EV_g\frac{2\pi\Delta f}{s} + \Delta EV_g\varphi\right) \tag{22}$$

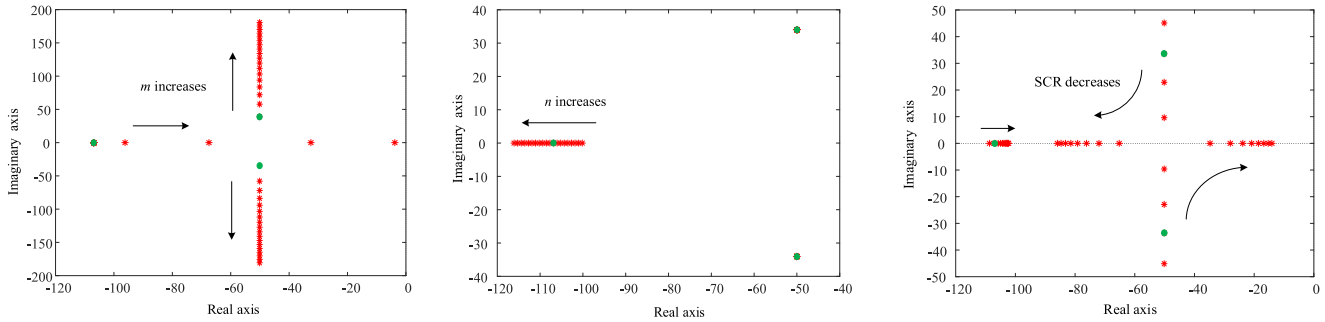

FIGURE 4. Root locus diagrams for the small-signal model. (a) Changing *m* with fixed *n*, (b) Changing *n* with fixed *m*, (c) Changing SCR with fixed *m* and *n*.

$$\Delta E = -\frac{nV_g\varphi}{Z_s(w_f + s)} \tag{23}$$

Where the symbol w_f represents the cut-off frequency of the low-pass filters. Based on (22) and (23), the characteristic equation can be derived as a third-order expression, as shown in (24).

$$a_3 s^3 + a_2 s^2 + a_1 s + a_0 = 0 \tag{24}$$

where

$$\begin{aligned} a_3 &= Z_s^2 \\ a_2 &= 2Z_s^2 w_f + nZ_s w_f (2E - V_g) \\ a_1 &= 2\pi Z_s w_f mEV_g + nZ_s w_f^2 (2E - V_g) + Z_s^2 w_f^2 \\ a_0 &= 2\pi Z_s w_f^2 mEV_g + 2\pi w_f^2 mnEV_g (2E - V_g) \end{aligned}$$

B. PARAMETER DESIGN CONSIDERING SYSTEM STABILITY

The stability analysis of the proposed control system, including the determination of its parameters, relies on the characteristic equation derived from small-signal stability analysis. This process involves the utilization of root locus diagrams to analyze the system stability and optimize its parameters. Specifically, the decoupler parameters $D_1 \sim D_4$ are set based on the derived coupling characteristic of the system as shown in (17). The droop coefficients of the DER can be tuned to achieve the desired power-sharing capability [18]. To investigate the impact on the control stability, the droop coefficients undergo continuous adjustments, and the corresponding root locus diagrams are generated, as illustrated in Fig. 4 (a) and (b). Fig. 4 (a) presents the eigenvalue trajectory (in red) with varying droop coefficient m, with arrows indicating the direction of eigenvalue evolution. Similarly, Fig. 4 (b) shows how the eigenvalues change with alterations in the droop coefficient n. In both cases, the eigenvalues remain within the left half-plane, indicating that droop parameters can be fine-tuned to achieve the desired power sharing while maintaining system stability. In this study, the droop coefficients m and n are set based on the P-f droop of 0.05 per unit (p.u.) and the Q-V droop of 0.1 p.u. after decoupling. The corresponding eigenvalues obtained with the specified m and n are illustrated in green in Fig. 4 (a) and (b).

Furthermore, to investigate the controller stability in the face of a heightened weakness in the distribution grid, the SCR of the weak distribution grid is systematically adjusted. As illustrated in Fig. 4 (c), the eigenvalue plot demonstrates the evolution as the SCR decreases continuously from 3.4 to 0.8 within the studied system. Notably, throughout this range, all the eigenvalues consistently reside in the left half plane, indicating that the proposed controller can maintain stability across different levels of grid weakness.

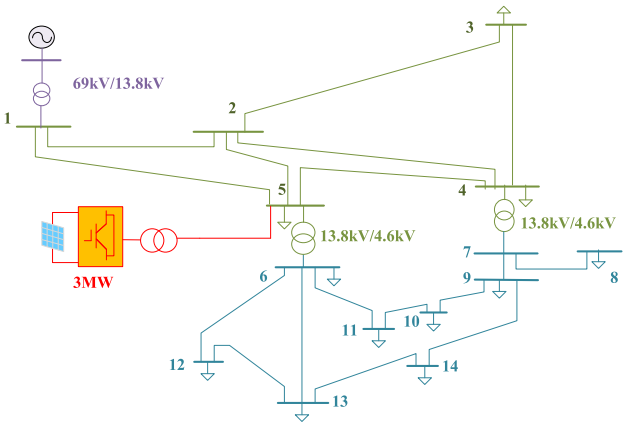

FIGURE 5. A weak distribution system based on IEEE 14 bus system.

IV. CASE STUDIES

To validate the proposed control scheme, thorough tests are carried out in a weakened distribution grid using MATLAB/Simulink and OPAL-RT. The weak grid model is constructed based on the IEEE 14-bus system, depicted in Fig. 5 [42].

The 14-bus weak distribution grid is connected to a swing bus (69kV) via a 13.8 kV/69 kV transformer at Bus 1. Voltage levels in this grid include 13.8 kV and 4.6 kV. A utility-scale DER with a capacity of 3 MVA is connected to Bus 5 via

TABLE 1. Simulation cases and specifications.

Cases	Description of scenarios
Case I	**Comparison of proposed systematic decoupling grid-forming control with non-decoupling droop-based grid-forming control**
Case I(A)	Simulation of f step reponse
Case I(B)	Simulation of V step reponse
Case II	**Comparison of proposed systematic decoupling grid-forming control with existing Z_{DER}-based decoupling grid-forming control in the system with varying R/X ratio**
Case II(A)	Simulation of f step response with R/X ratio of 1.45:1
Case II(B)	Simulation of V step response with R/X ratio of 1.45:1
Case II(C)	Simulation of f step response with R/X ratio of 1.72:1
Case II(D)	Simulation of V step response with R/X ratio of 1.72:1
Case III	**Comparison of proposed systematic decoupling grid-forming control with existing Z_{DER}-based decoupling grid-forming control in the system with unbalanced events and harmonics**
Case III(A)	Simulation of unbalanced events with R/X ratio of 1.45:1
Case III(B)	Simulation of unbalanced events with R/X ratio of 1.72:1
Case III(C)	Simulation of single-phase failure with R/X ratio of 1.72:1

a 480 V/13.8 kV transformer. The short-circuit capacity of the grid is set as 8.5 MVA, resulting in a low SCR of 2.83. For our study, we utilize the OPAL-RT real-time simulation platform, which includes the hardware simulator OP5600, real-time-based software RT-LAB, and phasor-domain software ePHASORSIM to facilitate real-time simulation. The detailed configuration process of this simulation setup is elaborated in [43].

The step responses to f and V disturbances in the control loop are conducted to validate the effectiveness of the independent f and V control by evaluating their mutual interferences. The decoupling performance of the proposed controller is compared with the traditional non-decoupling droop-based grid-forming control and the existing Z_{DER}-based decoupling grid-forming control. The comparison cases are outlined in TABLE 1.

To evaluate the stability and dynamic performance resulting from the decoupled P and Q, both f and V step responses are studied in this paper. It is noted that the f of the DER in the simulation cases does not instantaneously follow the f step-up reference change applied to the controller. This behavior aligns with the nature of a realistic power system, where frequency is a global variable that is dominated by the upstream transmission system. In addition, in Case II, the comparison cases are conducted in a system with a varying R/X ratio, aiming to analyze the decoupling performance of

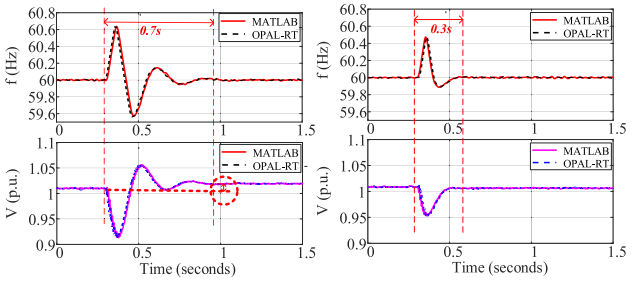

(a) Non-decoupling droop based grid-forming control (b) Proposed systematic decoupling grid-forming control

FIGURE 6. Case I (A): Simulation of f step response.

the proposed control against that of the existing Z_{DER}-based decoupling grid-forming control under different coupling characteristics.

A. CASE I: COMPARISON WITH NON-DECOUPLING DROOP-BASED GRID-FORMING CONTROL

Case I (A): Simulation of f step response. In this case, the f and V performance of a DER using the proposed control strategy is contrasted with a traditional control scheme under an identical condition, specifically a 2.5% f step change at 0.3 s. Their simulation results are shown in Fig. 6.

In Fig. 6 (a), the f step response of the DER using the non-decoupling grid-forming controller is presented. The results reveal an oscillatory and underdamped response, characterized by a substantial valley excursion and a settling time of 0.7 s. Importantly, the V fails to return to its nominal value in the steady state. This indicates that the V of the DER can be significantly impacted by f disturbances, potentially leading to inverter tripping. Concurrently, the f exhibits considerable oscillation due to the coupled nature of the traditional control. However, it eventually stabilizes at the nominal value, due to the swing bus mechanism. In Fig. 6 (b), the f and V performance of the DER using the proposed control is illustrated. Notably, after the f reference step change, the V experiences a better-damped response with a significantly reduced valley excursion compared to Fig. 6 (a). The V swiftly returns to the nominal value within 0.3 s. This behavior indicates that under the regulation of the proposed controller, the V of the DER remains stable and unaffected by the f reference step change. Therefore, the proposed control strategy effectively decouples f and V regulations. When compared to the traditional non-decoupling grid-forming control, the proposed control enables the DER to achieve independent V control, leading to a better-damped response and enhanced stability when the DER encounters a frequency disturbances.

Case I(B): Simulation of V step response. This case involves a comparison of the f and V performance of a DER using the proposed control strategy against the traditional control scheme under an identical V reference step change of 5% at 0.3 s. Their simulation results are presented in Fig. 7.

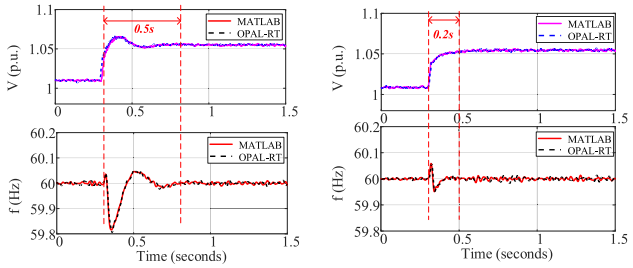

(a) Non-decoupling droop based grid-forming control (b) Proposed systematic decoupling grid-forming control

FIGURE 7. Case I (B): Simulation of V step response.

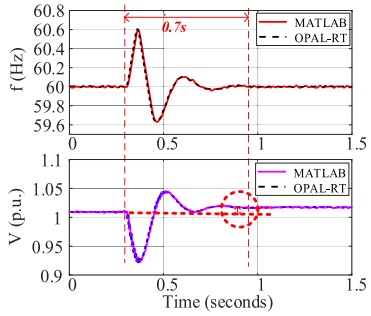

FIGURE 8. Case II (A): Simulation of f response of Z_{DER}-based grid-forming control with R/X ratio as 1.45:1.

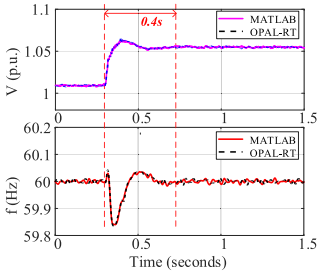

FIGURE 9. Case II (B): Simulation of V step response of Z_{DER}-based grid-forming control with R/X ratio as 1.45:1.

In Fig. 7 (a), the V step response using the non-decoupling droop-based grid-forming control is depicted. The results demonstrate that the V increases to 1.05 p.u. following the V reference step change. However, this increase is accompanied by a substantial overshoot and a settling time of 0.5 s. Simultaneously, the f is significantly influenced by the V step change, exhibiting considerable fluctuations that could potentially lead to load or inverter tripping. This observation indicates that the f performance is adversely affected by V disturbances. In contrast, Fig. 7 (b) showcases the f and V performance of the DER when operated under the proposed control strategy. The results reveal that the V of the DER increases to 1.05 p.u. within approximately 0.2 s without overshoot, demonstrating a fast and well-damped V response akin to a first-order system. Furthermore, it is seen that after the volage reference step change, the f excursion is almost entirely mitigated, and the resulting settling time is significantly reduced compared to Fig. 7 (a).

These observations clearly indicate that the dynamic performance of the proposed control is substantially superior to that of the traditional control scheme. In comparison to traditional control, the proposed control can dynamically decouple the entire system based on real-time measurements, reducing interference between frequency and voltage control. As a result, the proposed control strategy enables the DER to achieve independent f control and exhibit a better-damped response, thereby improving overall stability during V disturbances.

B. CASE II: COMPARISON WITH Z_{DER}-BASED DECOUPLING GRID-FORMING CONTROL

This section presents a comparative analysis of the f and V step responses between the proposed control and the existing Z_{DER}-based decoupling grid-forming control. The latter primarily focuses on decoupling the DER system and neglects the impact of grid coupling issues. To assess the decoupling performance of these control schemes in the power grid, different resistance-to-reactance (R/X) ratios (specifically, 1.45:1 and 1.72:1) of the system impedance are utilized. It is noteworthy that the performance of the DER using the proposed control with an R/X ratio of 1.45:1 was previously elaborated in Case I.

Case II(A): Simulation of f step response (R/X ratio of the entire system is 1.45:1). This case evaluates the f and V performance of the DER using the existing Z_{DER}-based decoupling grid-forming control during the same event as in Case I, namely a 2.5% f step change at 0.3 s. Fig. 8 illustrates the response of the DER using the existing Z_{DER}-based decoupling grid-forming control following the f step change.

It is seen in Fig. 8 that the f displays severe oscillatory and underdamped behavior, similar to that observed in Fig. 6 (a). The V experiences significant excursions and oscillations with a settling time of 0.7 s, failing to return to the nominal value. This outcome reveals that the Z_{DER}-based decoupling control falls short in effectively decoupling f and V regulation, as it does not consider the impact of the power grid on the DER control. In contrast, Fig. 6 (b) showcases the proposed control strategy, demonstrating significantly superior dynamic performance in comparison to the Z_{DER}-based decoupling control.

Case II(B): Simulation of V step response. (R/X ratio of the entire system is 1.45:1). This case evaluates the f and V performance of the DER using the existing Z_{DER}-based decoupling grid-forming control under a 5% V reference step change at 0.3 s. As shown in Fig. 9, the V increases to 1.05 p.u. following the step change with a settling time of 0.4 s. As observed, the f experiences a significant excursion and underdamped oscillation. Although the settling time is slightly shorter than the 0.5 s observed in Fig. 7 (a), it is notably longer than the response seen in Fig. 7 (b) with

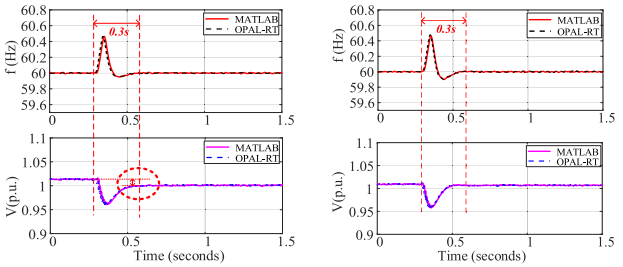

(a) Z_{DER}-based decoupling grid-forming cotnrol (b) Proposed systematic decoupling grid-forming control

FIGURE 10. Case II (C): Simulation of f step response with R/X ratio as 1.72:1.

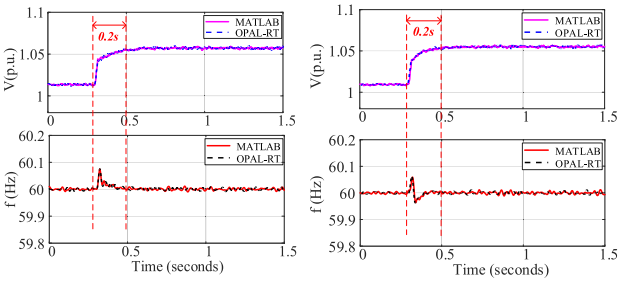

(a) Z_{DER}-based decoupling grid-forming control (b) Proposed systematic decoupling grid-forming control

FIGURE 11. Case II (D): Simulation of V step response with R/X ratio as 1.72:1.

the proposed control. This indicates that the existing Z_{DER}-based control cannot achieve accurate f control with good dynamic performance under V disturbances. In contrast, the DER using the proposed control strategy, as depicted in Fig. 7 (b), exhibits improved f and V control performance.

It is important to highlight that, much like the traditional non-decoupling droop-based control, the existing Z_{DER}-based decoupling control shows inferior f and V control performance compared to the proposed control strategy under disturbances. Despite its consideration of the coupling issue, the Z_{DER}-based decoupling control solely focuses on the decoupling of the output impedance of the DER system, namely, Z_{DER}, which encompasses only the impedances of the filter and outlet line. Furthermore, this Z_{DER}-based control approach treats the power grid as an ideal voltage source. As a result, the Z_{DER}-based decoupling control approach proves inadequate in weak grids characterized by substantial grid impedance, especially when the R/X ratio of Z_{DER} markedly differs from that of the grid impedance.

Case II(C): Simulation of f step response (R/X ratio of the entire system is 1.72:1). To further explore the decoupling performance, the R/X ratio of the system impedance is changed from 1.45:1 to 1.72:1. This case compares the f and V performance of the DER using the proposed control against the existing Z_{DER}-based control under a 2.5% f reference step change. Fig. 10 (a) shows the f step response of the DER using the Z_{DER}-based control. The V has a minor excursion with a settling time of 0.3 s after the f reference step change is applied. However, it does not return to the nominal value after the fluctuation, indicating its susceptibility to the f reference step change. In contrast, Fig. 10 (b) displays the f and V performance of the DER using the proposed control. It is seen that the proposed control effectively eliminates the impact of f disturbances on the V response, showcasing a notable improvement over the results observed in Fig. 10 (a).

Case II(D): Simulation of V step response (R/X ratio of the entire system is 1.72:1). This case compares the f and V performance of the DER using the proposed control with that using the existing Z_{DER}-based control under a 5% V step change. Fig. 11 (a) illustrates the V step response of the DER with the Z_{DER}-based control.

It exhibits improved performance compared to Case II (B) in Fig. 9, where the DER utilizes the Z_{DER}-based control with a power grid R/X ratio of 1.45:1. This enhancement is attributed to the adjustment of the R/X ratio of the entire system impedance closer to the output impedance of the DER. This adjustment enables the Z_{DER}-based control to perform better under the V disturbance. However, the f step response in Fig. 11 (a) indicates that this control method is unable to completely mitigate the impact of the V disturbance on f regulation. Fig. 11 (b) demonstrates the simulation results using the proposed control. It is seen that there is a reduction in the settling time for f with reduced excursion and the f returns to the nominal value more quickly.

Furthermore, the f and V step responses of the proposed control in Fig. 10 (b) and 11 (b), closely resemble those in Fig. 6 (b) and 7 (b). This indicates that the proposed control strategy can consistently maintain independent and well-damped f and V regulation in a power grid, even with varying coupling characteristics.

C. CASE III: COMPARISON WITH Z_{DER}-BASED DECOUPLING GRID-FORMING CONTROL UNDER UNBALANCED EVENTS AND HARMONICS

In this study, we compare the f and V responses of the proposed control with those of the existing Z_{DER}-based control under unbalanced operational conditions. These conditions are typically caused by unbalanced loads or unsymmetrical faults and are known to induce harmonics and stability challenges. We simulate these scenarios by adjusting the voltage magnitude of Phase A at predetermined intervals, effectively reproducing the dynamics and harmonic impacts of unbalanced operations. The primary objective is to evaluate the effectiveness of the proposed decoupler in enhancing f and V stability. It is important to note that additional control function designs, such as the FRT and sequence control of the DER, are beyond the scope of this paper.

Case III(A): Simulation of unbalanced events (R/X ratio of the entire system is 1.45:1). This case investigates the f and V performance under a specific scenario: variation in the voltage amplitude of Phase A. This variation includes modifying the V magnitude of Phase A to 0.8 p.u. at 0.3 s,

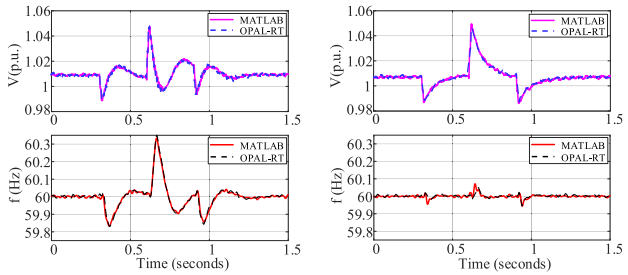

(a) Z_{DER}-based decoupling grid-forming cotnrol (b) Proposed systematic decoupling grid-forming control

FIGURE 12. Case III (A): Simulation of an unbalanced event with R/X ratio as 1.45:1.

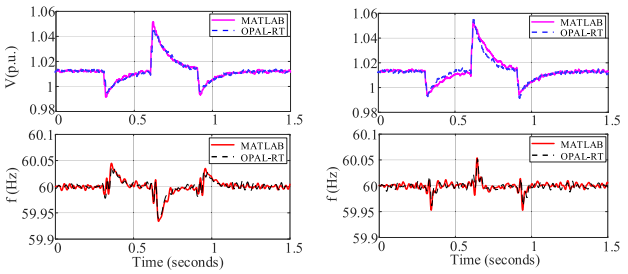

(a) Z_{DER}-based decoupling grid-forming control (b) Proposed systematic decoupling grid-forming control

FIGURE 13. Case III (B): Simulation of an unbalanced event with R/X ratio as 1.72:1.

1.2 p.u. at 0.6 s, and 1.0 p.u. at 0.9 s. Fig.12 (a) presents the response of the DER when applying the Z_{DER}-based control. It reveals an oscillatory f and V response with significant deviations, which may lead to inverter tripping during unbalanced conditions.

Fig 12 (b) illustrates the response of the DER when utilizing the proposed control method. In contrast to Fig. 12 (a), Fig. 12 (b) displays enhanced f and V performance of the DER. It is seen that the V response is more effectively damped, rapidly returning to the nominal value unlike the scenario depicted in Fig. 12 (a). The f shows fewer oscillations compared to the Z_{DER}-based control, indicating that the proposed control scheme has better stabilization capability than the existing Z_{DER}-based control schemes during unbalanced events.

Case III(B): Simulation of unbalanced events (R/X ratio of the entire system is 1.72:1). This case examines the f and V performance of the DER using the proposed control in comparison to the Z_{DER}-based control under the same event as in Case III (A) but with the R/X ratio of the entire system changed to 1.72:1. As observed, Fig. 13 (a) shows improved f and V performance under the Z_{DER}-based control compared to Fig. 12 (a) in Case III (A), where the power grid R/X ratio is 1.45:1. As discussed in Case II (D), this f and V response improvement is attributed to the closer matching of the R/X ratio of the entire system impedance to the output impedance of the DER. Importantly, Fig. 13 (b) shows the f and V performance of the DER using the proposed control. It exhibits

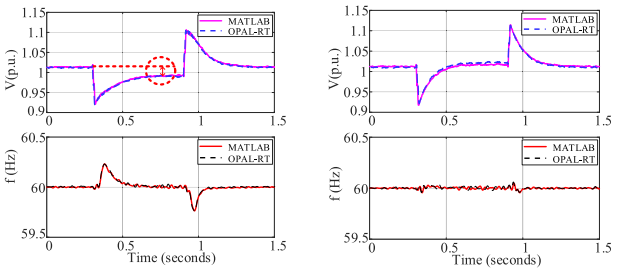

(a) Z_{DER}-based decoupling grid-forming cotnrol (b) Proposed systematic decoupling grid-forming control

FIGURE 14. Case III (C): Simulation of a single-phase fault with R/X ratio as 1.72:1.

better f and V dynamics than Fig. 13 (a), characterized by a reduced excursion and shorter settling time.

Case III(C): Simulation of single-phase failure (R/X ratio of the entire system is 1.72:1). This case compares the f and V performance of a DER using the proposed control with that using the Z_{DER}-based control during a single-phase fault. The fault is performed by modifying the V magnitude of Phase A to 0 from 0.3 s to 0.9 s. Fig. 14 (a) displays the f and V response of the DER using the Z_{DER}-based control.

As seen in Fig. 14 (a), the V experiences a noticeable excursion and does not return to the nominal value. This indicates that the Z_{DER}-based control degrades the steady-state performance during an unbalanced fault. Meanwhile, the f in Fig. 14 (a) has a large deviation and a long settling time of around 0.2 s. Conversely, Fig. 14 (b) shows that using the proposed control scheme has a lesser impact on f dynamics and results in a rapid V recovery to the nominal value, effectively mitigating the impact of the unbalanced fault compared to Fig. 14 (a).

Case III conclusively demonstrates the superior performance of the proposed control over the Z_{DER}-based control in regulating f and V in weak distribution grids. It delivers enhanced dynamic responses, steady-state performance, and superior system stabilization under unbalanced conditions.

V. CONCLUSION

This paper proposes a robust and unified systematic decoupling grid-forming control scheme for the DER operating in weak distribution grids. The primary objective is to significantly enhance dynamic response and stability performance. In contrast to existing DER grid-forming control methods that often treat distribution grids as a simple Thevenin equivalent circuit, the proposed controller is designed from a system-wide perspective, taking into consideration the coupling characteristics of the entire power grid. The simulation results demonstrate that the developed control strategy can enable DERs to decouple P and Q and regulate f and V independently. In conclusion, this proposed control strategy offers several advantages: (1) easy commercialization and market promotion due to its simple and robust circuit design; (2) provision of a unified grid-forming controller for DERs,

TABLE 2. Parameters and system settings.

Parameter	Symbol	Value
Voltage setpoint	E_0	480 V
Nominal frequency	f_0	60 Hz
Active power setpoint	P_o	1 MW
Reactive power set point	Q_0	0 kVar
DC voltage of DER	V_{dc}	850 V
Cut off frequency	w_f	100 rad/s

simplifying various operating modes outlined in IEEE Standard 1547-2018, particularly in addressing coupled P and Q issues; and (3) elimination of the need for communication links between DERs, reducing costs and minimizing the risk of cyber-attacks.

It is important to note that this paper specifically focuses on the systematic decoupling control design of the DER. Coordination among multiple DERs in a grid and the optimization of the operation are beyond the scope of this work and will be explored in future research. Further insight and advancements in this domain will be presented in forthcoming papers.

APPENDIX

See Table 2.

ACKNOWLEDGMENT

The authors would like to thank Shuaiang Rong for editing a portion of the manuscript.

REFERENCES

[1] *Act (CLEAN Future Act)*, Senate House Representatives United States Amer., Washington, DC, USA, Mar. 2021.

[2] *United States Distributed Energy Resources Outlook: DER Installations and Forecasts 2016-2025E*, Wood Mackenzie, Louisville, KY, USA, Jun. 2020.

[3] B. Kroposki et al., "Achieving a 100% renewable grid: Operating electric power systems with extremely high levels of variable renewable energy," *IEEE Power Energy Mag.*, vol. 15, no. 2, pp. 61–73, Mar. 2017.

[4] E. Rehman, M. G. Miller, J. Schmall, S. H. Huang, and J. Billo, "Stability assessment of high penetration of inverter-based generation in the ERCOT grid," in *Proc. IEEE Power Energy Soc. Gen. Meeting (PESGM)*, Atlanta, GA, USA, Aug. 2019, pp. 1–5.

[5] *Black System South Australia 28 September 2016-Final Report*, Austral. Energy Market Operator, Sydney, NSW, Australia, Mar. 2017.

[6] *9 August 2019 Power Outage Report*, Office Gas Electr. Markets (Ofgem), London, U.K., Jan. 2020.

[7] X. Chen, Y. Zhang, S. Wang, J. Chen, and C. Gong, "Impedance-phased dynamic control method for grid-connected inverters in a weak grid," *IEEE Trans. Power Electron.*, vol. 32, no. 1, pp. 274–283, Jan. 2017.

[8] I. Hussain, R. K. Agarwal, and B. Singh, "MLP control algorithm for adaptable dual-mode single-stage solar PV system tied to three-phase voltage-weak distribution grid," *IEEE Trans. Ind. Informat.*, vol. 14, no. 6, pp. 2530–2538, Jun. 2018.

[9] *IEEE Standard for Interconnection and Interoperability of Distributed Energy Resources With Associated Electric Power Systems Interfaces*, Standard 1547-2018, Revision of IEEE Standard 1547-2003, 2018, pp. 1–138.

[10] S. C. Ross, G. Vuylsteke, and J. L. Mathieu, "Effects of load-based frequency regulation on distribution network operation," *IEEE Trans. Power Syst.*, vol. 34, no. 2, pp. 1569–1578, Mar. 2019.

[11] J. Rocabert, A. Luna, F. Blaabjerg, and P. Rodríguez, "Control of power converters in AC microgrids," *IEEE Trans. Power Electron.*, vol. 27, no. 11, pp. 4734–4749, Nov. 2012.

[12] Y. Sun, S. Bahrami, V. W. S. Wong, and L. Lampe, "Chance-constrained frequency regulation with energy storage systems in distribution networks," *IEEE Trans. Smart Grid*, vol. 11, no. 1, pp. 215–228, Jan. 2020.

[13] L. Sang, Y. Xu, W. Wu, and H. Long, "Online voltage regulation of active distribution networks: A deep neural encoding-decoding approach," *IEEE Trans. Power Syst.*, early access, Sep. 2023.

[14] W. Alabri and D. Jayaweera, "Voltage regulation in unbalanced power distribution systems with residential PV systems," *Int. J. Electr. Power Energy Syst.*, vol. 131, Oct. 2021, Art. no. 107036.

[15] P. Kundur, *Power System Stability and Control*, 1st ed. New York, NY, USA: McGraw-Hill, 1994.

[16] L. He, C.-C. Liu, A. Pitto, and D. Cirio, "Distance protection of AC grid with HVDC-connected offshore wind generators," *IEEE Trans. Power Del.*, vol. 29, no. 2, pp. 493–501, Apr. 2014.

[17] D. Pattabiraman, R. H. Lasseter., and T. M. Jahns, "Comparison of grid following and grid forming control for a high inverter penetration power system," in *Proc. IEEE Power Energy Soc. Gen. Meeting (PESGM)*, Portland, OR, USA, Aug. 2018, pp. 1–5.

[18] W. Du, Q. Jiang, M. J. Erickson, and R. H. Lasseter, "Voltage-source control of PV inverter in a CERTS microgrid," *IEEE Trans. Power Del.*, vol. 29, no. 4, pp. 1726–1734, Aug. 2014.

[19] Q.-C. Zhong and G. Weiss, "Synchronverters: Inverters that mimic synchronous generators," *IEEE Trans. Ind. Electron.*, vol. 58, no. 4, pp. 1259–1267, Apr. 2011.

[20] M. Sinha, F. Dörfler, B. B. Johnson, and S. V. Dhople, "Virtual oscillator control subsumes droop control," in *Proc. Amer. Control Conf. (ACC)*, Jul. 2015, pp. 2353–2358.

[21] D. Çelik and M. E. Meral, "A coordinated virtual impedance control scheme for three phase four leg inverters of electric vehicle to grid (V2G)," *Energy*, vol. 246, May 2022, Art. no. 123354.

[22] J. He, L. Du, B. Liang, Y. Li, and C. Wang, "A coupled virtual impedance for parallel AC/DC converter based power electronics system," *IEEE Trans. Smart Grid*, vol. 10, no. 3, pp. 3387–3400, May 2019.

[23] B. Wei, Y. Gui, S. Trujillo, J. M. Guerrero, J. C. Vásquez, and A. Marzàbal, "Distributed average integral secondary control for modular UPS systems-based microgrids," *IEEE Trans. Power Electron.*, vol. 34, no. 7, pp. 6922–6936, Jul. 2019.

[24] M. Pham and H. Lee, "Coordinated virtual resistance and capacitance control scheme for accurate reactive power sharing and selective harmonic compensation in islanded microgrid," *IET Gener., Transmiss. Distrib.*, vol. 14, no. 22, pp. 5104–5113, Sep. 2020.

[25] Y. Han, P. Shen, X. Zhao, and J. M. Guerrero, "Control strategies for islanded microgrid using enhanced hierarchical control structure with multiple current-loop damping schemes," *IEEE Trans. Smart Grid*, vol. 8, no. 3, pp. 1139–1153, May 2017.

[26] M.-D. Pham and H.-H. Lee, "Effective coordinated virtual impedance control for accurate power sharing in islanded microgrid," *IEEE Trans. Ind. Electron.*, vol. 68, no. 3, pp. 2279–2288, Mar. 2021.

[27] M. Karimi-Ghartemani, S. A. Khajehoddin, P. Piya, and M. Ebrahimi, "Universal controller for three-phase inverters in a microgrid," *IEEE J. Emerg. Sel. Topics Power Electron.*, vol. 4, no. 4, pp. 1342–1353, Dec. 2016.

[28] I. Sadeghkhani, M. E. H. Golshan, A. Mehrizi-Sani, and J. M. Guerrero, "Low-voltage ride-through of a droop-based three-phase four-wire grid-connected microgrid," *IET Gener. Transm. Distrib.*, vol. 12, no. 8, pp. 1906–1914, Apr. 2018.

[29] B. Pawar, E. I. Batzelis, S. Chakrabarti, and B. C. Pal, "Grid-forming control for solar PV systems with power reserves," *IEEE Trans. Sustain. Energy*, vol. 12, no. 4, pp. 1947–1959, Oct. 2021.

[30] S. Yu, S. Rong, and L. He, "Performance of grid-forming control of grid-edge DERs in distribution grids," in *Proc. IEEE Power Energy Soc. Gen. Meeting (PESGM)*, Denver, CO, USA, Jul. 2022, pp. 1–5.

[31] A. Moawwad, V. Khadkikar, and J. L. Kirtley, "A new P-Q-V droop control method for an interline photovoltaic (I-PV) power system," *IEEE Trans. Power Del.*, vol. 28, no. 2, pp. 658–668, Apr. 2013.

[32] W. Yao, M. Chen, J. Matas, J. M. Guerrero, and Z.-M. Qian, "Design and analysis of the droop control method for parallel inverters considering the impact of the complex impedance on the power sharing," *IEEE Trans. Ind. Electron.*, vol. 58, no. 2, pp. 576–588, Feb. 2011.

[33] Q.-C. Zhong and Y. Zeng, "Universal droop control of inverters with different types of output impedance," *IEEE Access*, vol. 4, pp. 702–712, 2016.

[34] Z. Peng et al., "Droop control strategy incorporating coupling compensation and virtual impedance for microgrid application," *IEEE Trans. Energy Convers.*, vol. 34, no. 1, pp. 277–291, Mar. 2019.
[35] Y. Li and Y. W. Li, "Power management of inverter interfaced autonomous microgrid based on virtual frequency-voltage frame," *IEEE Trans. Smart Grid*, vol. 2, no. 1, pp. 30–40, Mar. 2011.
[36] J. Sun, "Impedance-based stability criterion for grid-connected inverters," *IEEE Trans. Power Electron.*, vol. 26, no. 11, pp. 3075–3078, Nov. 2011.
[37] K. V. Kkuni, M. Nuhic, and G. Yang, "Power system stability impact assessment for the current limits of grid supporting voltage-source converters," in *Proc. IEEE Power Energy Soc. Gen. Meeting (PESGM)*, Jul. 2021, pp. 1–5.
[38] E. Zhao, Y. Han, X. Lin, P. Yang, F. Blaabjerg, and A. S. Zalhaf, "Impedance characteristics investigation and oscillation stability analysis for two-stage PV inverter under weak grid condition," *Electr. Power Syst. Res.*, vol. 209, Aug. 2022, Art. no. 108053.
[39] S. Bennai, A. B. Abdelghani, I. Slama-Belkhodja, and M. Khalfoun, "Sensitivity analysis to grid line impedance for grid characterization and stability assessment investigations," in *Proc. IEEE Int. Conf. Electr. Sci. Technol. Maghreb (CISTEM)*, vol. 4, Tunis, Tunisia, Oct. 2022, pp. 1–6.
[40] *IEEE Guide for Planning DC Links Terminating At AC Locations Having Low Short-circuit Capacities*, IEEE Standard 1204-1997, Jan. 1997, pp. 1–216.
[41] J. C. Vasquez, J. M. Guerrero, A. Luna, P. Rodriguez, and R. Teodorescu, "Adaptive droop control applied to voltage-source inverters operating in grid-connected and islanded modes," *IEEE Trans. Ind. Electron.*, vol. 56, no. 10, pp. 4088–4096, Oct. 2009.
[42] *IEEE 14 Bus System*. Accessed: Feb. 1, 2022. [Online]. Available: http://labs.ece.uw.edu/pstca/pf14/pg_tca14bus.htm
[43] S. S. Noureen, V. Roy, and S. B. Bayne, "An overall study of a real-time simulator and application of RT-LAB using MATLAB simpowersystems," in *Proc. IEEE Green Energy Smart Syst. Conf. (IGESSC)*, Long Beach, CA, USA, Nov. 2017, pp. 1–5.

LINA HE (Senior Member, IEEE) received the B.S. and M.S. degrees from the Huazhong University of Science and Technology, China, in 2007 and 2009, respectively, and the Ph.D. degree in electrical engineering from University College Dublin, Ireland, in 2014. From 2014 to 2017, she was the Project Manager and a Senior Consultant at Siemens Headquarters, Germany, and Siemens, USA. She is currently an Assistant Professor with the Department of Electrical and Computer Engineering, University of Illinois at Chicago, Chicago, IL, USA. Her research interests include modeling, control, and protection of power electronics-based power systems, renewable energy integration, HVdc control and operation, and wide-area protection and cybersecurity.

SHIWEN YU (Graduate Student Member, IEEE) received the B.S. and M.S. degrees in electrical engineering from the Wuhan University of Technology, in 2017 and 2020, respectively. He is currently pursuing the Ph.D. degree in electrical engineering with the University of Illinois at Chicago, Chicago, IL, USA. His research interests include grid-forming control, power systems stability, and machine learning.